NUCL SCI TECH (2019) 30:81
https://doi.org/10.1007/s41365-019-0608-0

An APXPS endstation for gas–solid and liquid–solid interface studies at SSRF

Jun Cai[1,2,3] · Qiao Dong[1,3] · Yong Han[2] · Bao-Hua Mao[1] · Hui Zhang[1] · Patrik G. Karlsson[4] · John Åhlund[4] · Ren-Zhong Tai[5] · Yi Yu[2] · Zhi Liu[1,2]

Received: 26 March 2019 / Revised: 4 April 2019 / Accepted: 4 April 2019 / Published online: 13 April 2019

Abstract In the past few decades, various surface analysis techniques find wide applications in studies of interfacial phenomena ranging from fundamental surface science, catalysis, environmental science and energy materials. With the help of bright synchrotron sources, many of these techniques have been further advanced into novel in-situ/*operando* tools at synchrotron user facilities, providing molecular level understanding of chemical/electrochemical processes in-situ at gas–solid and liquid–solid interfaces. Designing a proper endstation for a dedicated beamline is one of the challenges in utilizing these techniques efficiently for a variety of user's requests. Many factors, including pressure differential, geometry and energy of the photon source, sample and analyzer, need to be optimized for the system of interest. In this paper, we discuss the design and performance of a new endstation at beamline 02B at the Shanghai Synchrotron Radiation Facility for ambient pressure X-ray photoelectron spectroscopy studies. This system, equipped with the newly developed high-transmission HiPP-3 analyzer, is demonstrated to be capable of efficiently collecting photoelectrons up to 1500 eV from ultrahigh vacuum to ambient pressure of 20 mbar. The spectromicroscopy mode of HiPP-3 analyzer also enables detection of photoelectron spatial distribution with resolution of 2.8 ± 0.3 μm in one dimension. In addition, the designing strategies of systems that allow investigations in phenomena at gas–solid interface and liquid–solid interface will be highlighted through our discussion.

Keywords Ambient pressure XPS · Synchrotron · Liquid–solid interface · Spectromicroscopy

Jun Cai, Qiao Dong and Yong Han have contributed equally in this work.

This work was supported by the National Natural Science Foundation of China (No. 11227902) as part of NSFC ME^2 beamline project and Science and Technology Commission of Shanghai Municipality (No. 14520722100). Y.H., Y.Y., and B.M. are supported by National Natural Science Foundation of China (Nos. 21802096, 21832004, and 11805255).

✉ Yi Yu
yuyi2@shanghaitech.edu.cn

✉ Zhi Liu
zliu2@mail.sim.ac.cn

[1] State Key Laboratory of Functional Materials for Informatics, Shanghai Institute of Microsystem and Information Technology, Chinese Academy of Sciences, Shanghai 200050, China

[2] School of Physical Science and Technology, ShanghaiTech University, Shanghai 201210, China

[3] University of Chinese Academy of Sciences, Beijing 100049, China

[4] Scienta Omicron, Uppsala 75228, Sweden

[5] Shanghai Institute of Applied Physics, Chinese Academy of Sciences, Shanghai Synchrotron Radiation Facility, Shanghai 201800, China

1 Introduction

Obtaining a molecular level understanding of phenomena at gas–solid interface and liquid–solid interface is of significant importance not only for fundamental scientific perspective but also for practical concerns to improve the efficiency and durability of chemical/electrochemical systems. The chemical, geometrical and electronic properties of these interfaces have a strong impact on the elementary processes, including adsorption/desorption, charge transfer

and formation/cleavage of chemical bonds and thus play a key role in determining the entire reaction mechanism [1]. This drives tremendous efforts in the past few decades to apply surface analysis techniques in investigations of interfacial structures and related phenomena. In this context, photoelectron spectroscopy (PES) stands as one of the most valuable and widely used characterization techniques. We would first provide a brief overview on the development of PES from ex-situ vacuum measurements to in-situ gas–solid studies at synchrotron facilities. An elaborated discussion on designing strategies of synchrotron-based investigation systems is given and then followed by with examples. Lastly, we present a description of our newly built APXPS endstation at SSRF with a high-transmission analyzer as well as its performance evaluation under ambient pressures up to 20 mbar, which demonstrates the capabilities of this system for gas–solid and liquid–solid studies in-situ/*operando*.

PES is a powerful analytical technique in probing the surface compositions and chemical states of elements in materials [2]. Its surface sensitivity originates from the strong interactions of the photoelectrons with matters, which is characterized by the short (nm-scale) inelastic mean free path of photoelectrons in solid or liquid [3]. Due to its surface sensitivity and same strong interactions of photoelectrons with gas molecules, this technique has traditionally been limited in UHV environments. Such ex-situ PES measurements (e.g., sample characterizations in vacuum before and after a reaction or gas exposure) have greatly improved our understanding of many catalytic systems in early days of this technique [4]. However, whether those measurements could accurately reveal the true fundamental chemistries of the interfaces remains a concern. Many interesting catalytic processes or adsorption phenomena at interfaces under realistic working conditions could hardly be captured in conventional vacuum PES studies. This is the so-called "pressure gap", i.e., the discrepancy of materials between UHV in surface science experiments and the much higher pressures relevant to practical catalyst applications [5, 6].

In order to bridge the pressure gap, continuous efforts have been made over the past 50 years toward achieving PES measurements at elevated pressures. In 1969, K. Siegbahn et al. designed the first photoelectron spectrometer for gas-phase experiments [7]. The basic concept is to minimize the distance, and the photoelectrons must travel in elevated-pressure region by separating the sample region from the electron spectrometer through a differentially-pumped aperture. A number of groups have followed this approach and have obtained, with varied instrument designs, photoemission measurements at up to $\sim$ 1 mbar [8–10]. To distinguish from conventional vacuum-based X-ray photoelectron spectroscopy, this technique is referred to as APXPS. However, an important compromise between the differential pumping and the photoelectron detection efficiency exists in these designs: a smaller aperture gives larger pressure differentials but on the other hand reduces the effective sample area. The diverging nature of the photoelectrons after emission poses another significant limitation on the transmission of photoelectrons through the analyzer. To overcome these challenges, Ogletree et al. integrated a differential pumping system with electrostatic lenses as a prototype instrument in 2002 [11]. With the electrostatic lenses, the photoelectrons are focused onto the differentially-pumped apertures so that differential pumping could be obtained while the photoemission signal is mostly preserved. This is also believed to be the first synchrotron-based APXPS system, demonstrating an upper pressure limit of 7 mbar. The second generation of APXPS instruments, taking advantage of the tightly focused and intense X-rays available at the high-brightness third-generation synchrotrons, has further increased the working pressure limit to $\sim$ 10 mbar through the use of smaller apertures [12, 13]. Since then, many APXPS systems have been built at different synchrotron facilities [11, 12, 14–17], while laboratory-based instruments with fixed X-ray sources become more readily available from commercial manufacturers. These rapid developments in APXPS experimental setups have greatly advanced our detection capabilities and, by providing invaluable in-situ information, play a critical role in our understanding of complex systems, especially those under relevant reaction conditions [3, 18–22].

While synchrotron-based APXPS is experiencing rapid growth around the world for in-situ/*operando* studies in various catalysis systems, it is worth mentioning that this achievement should not be considered as just a simple combination of the two technologies. A rational design of the APXPS endstation, which takes into account the specifics of a dedicated beamline and the scientific goals for systems of interest, is a crucial prerequisite. This is essential for experimentalists and beamline users since setups/geometries of an endstation might affect their experimental approaches or introduce side effects or even undesired results. By providing a discussion on the challenges and strategies in designing an endstation, specifically for gas–solid and liquid–solid APXPS investigations, we hope to highlight the necessity of a coordinated design for realizing the full capabilities offered by the light source and the analysis tool and more importantly to reveal possibilities in providing tailored solutions that aim for key questions in energy materials and conversion researches. Here, we discuss a few examples to illustrate how an optimal performance of a given system is achieved by a coordinated integration of the X-ray source, the differentially-pumped electron spectrometer, the experimental

system and the sample manipulation for various experimental goals.

Following the first prototype of differentially-pumped electrostatic lens and developments by Ogletree et al. [11, 12] beamline 9.3.2 at the Advanced Light Source (ALS) was further upgraded toward better performance. To match the large spot size of the beamline, a relatively large aperture diameter (0.85 mm) was chosen for maximizing photoelectron counts [14]. In such a case, the cone was specifically designed with a larger half-angle (60°) and thin aperture edge so that the gas would rapidly expand after crossing the aperture plane, giving an improved differential pumping performance. To improve the electron transmission and detection efficiency, the Scienta R4000 HiPP system was developed as a result of the collaboration between the ALS and its industrial partner. This system also featured an imaging capability with 16 μm spatial resolution in one dimension.

Another example is the APXPS design at beamline 9.3.1 at the ALS for solid–liquid interface studies. The tender X-ray (2–7 keV) available at this beamline was proven as an optimal photon energy range for such studies because one could ensure the photoelectrons energetic enough to penetrate through the liquid layer while the relative sensitivity to the key thin interface region maintained [21, 23]. Hence, the ability to efficiently detect photoelectrons with high kinetic energies creates a thin liquid film layer, and the ability to operate under higher pressures (up to 110 Torr) becomes the design criteria of the APXPS system. By introducing a shaped mesh as one of the lens elements in the pre-lens, the HiPP-2 analyzer was modified for detecting high kinetic energy (KE) electrons under high-pressure environments [23, 24].

In the next section, we present the design of a new APXPS endstation at beamline 02B at the SSRF, which serves as a third example of the designing strategies. This new bending magnet (BM) beamline delivers soft X-ray photon with a tightly focused beam spot size. With the new HiPP-3 analyzer, this system has successfully achieved high electron transmission and detection efficiency under gas pressures up to 30 mbar. The wide pressure range covered by this endstation enables studies of not only gas–solid systems, but also aqueous solutions and liquid–solid systems. Furthermore, the imaging capability has achieved a spatial resolution of 2.8 ± 0.3 μm in one dimension, well improved over the original HiPP system. This provides the opportunities to push the spectromicroscopy capability of APXPS system into micron range. A detailed description of the system and its performance evaluation is given below.

2 System overview

2.1 Endstation design

The APXPS endstation is connected to the BM beamline 02B at the SSRF. The BM section has a magnetic field of 1.27 *T* and a bending radius of 9.19 m. An energy range of 40–2000 eV is covered with three gratings: 400 l/mm, 800 l/mm and 1100 l/mm for the energies of 40–600 eV, 200–1600 eV and 200–2000 eV, respectively. For instance, a photon flux of 4×10^{10}–1×10^{11} photons/sec/0.1% bandwidth can be obtained below 1500 eV with 800 l/mm grating. The maximum energy resolving powers of this beamline is ~ 13,000 and the typical spot size is ~ 120 μm (H) × 15 μm (V).

In general, this endstation consists of four main parts: a load lock chamber, a preparation chamber, a μ-metal analysis chamber and the photoelectron analyzer (shown in Fig. 1a). The preparation chamber is equipped with an ion sputter gun (SPECS, IQE 11/35) and a three-grid low-energy electron diffraction optics (OCI, BDL600IR-3GR). Sample temperatures could be controlled in the range of 70–2000 K through a specially designed manipulator (FERMION Instruments (Shanghai) Co., Ltd). Spare ports are available for future installation of various evaporators, gas inlets and/or user equipment for in-situ sample preparation and pretreatment before APXPS measurements in the analysis chamber.

The analysis chamber is equipped with a four-axis manipulator system which consists of a home-built manipulator, an XYZ stage (Vacgen, Certiax) and a differentially-pumped rotary platform (Thermionics, RNN-400). Water cooling of the manipulator is employed to maintain its temperature and avoid thermal deformation during cooling and heating experiments. The sample holder (Thermionics, STLC platen) could be modified with a ceramic-coated button heater or Peltier heating/cooling unit. An infrared laser heating unit (PREVAC) is also mounted for catalytic systems to remove undesired background reactions [12, 25]. Additionally, the sample holder can accommodate up to four electrical connections for electrochemical measurements. During the ambient pressure experiment, the analysis chamber can be backfilled and controlled using UHV leak valves and its pressures can be monitored from 10^{-10} mbar to 110 mbar by a combination of an ion gauge (Agilent, UHV-24p) and two capacitance diaphragm gauges (Pfeiffer, CMR362 and CMR365).

To separate the ambient pressures in the analysis chamber from the beamline UHV environment, a silicon nitride (Si_3N_4) window (2 mm × 2 mm, thickness 100 nm) is mounted at the end of the beam port (Fig. 1b).

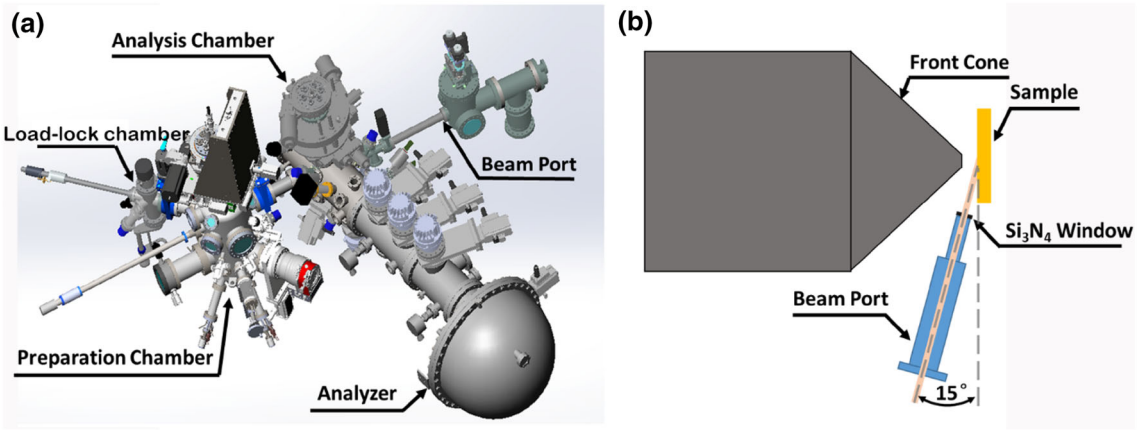

Fig. 1 (Color online) Schematics of the APXPS instrument at beamline 02B at the SSRF. **a** The system consists of four parts: a load lock chamber, a preparation chamber, a μ-metal analysis chamber and the Scienta analyzer. **b** The beamline with a 15° incident angle to the sample surface is separated by a Si_3N_4 window from the analysis chamber

This Si_3N_4 window allows 93% transmittance at 1000 eV photon energy. The beam port is tapered off for closer access to the sample ($\sim$ 30 mm) to reduce X-ray attenuation through the gas atmosphere. The incident angle of 15° (Fig. 1b) gives an elongated X-ray beam projection of $\sim$ 460 μm (H) $\times$ 15 μm (V) on the sample, matching well with the size of the front apertures (0.3 mm, 0.5 mm and 0.8 mm in diameter). With an aperture 0.3 mm in diameter, the differential pumping system could sustain a pressure up to 30 mbar in the analysis chamber while maintaining a $< 10^{-7}$ mbar pressure in the analyzer. This is close to the vapor pressure of water, the most common solvent in nature, at room temperature and thus enables a spectrum of new studies in liquid–solid interface besides the typical gas–solid interface measurements. Several design features of the previous HiPP-2 system, such as "dip & pull" setup, easy sample transfer and good adaptability for varied electrochemical setups, are also adopted in this system design [23].

In our first report of the "dip & pull" experiment, we have demonstrated that the liquid–solid interface could be probed efficiently through a thin liquid film ($\sim$ 10–30 nm) with tender X-ray source [23]. A recent study shows that this same method and detection efficiency could be extended to the soft X-ray region through a liquid film thinner than 10 nm [26]. We thus could perform liquid–solid interface studies at this BM beamline with our new APXPS endstation designed to carry out experiments as such.

2.2 Analyzer

The key component of this endstation is a Scienta Omicron HiPP-3 analyzer. From the first HiPP analyzer to the HiPP-2 analyzer and to this new HiPP-3 analyzer, the continual development path well depicts the essence of advanced instrument designs: different beamline specifics and different scientific goals usually require different strategies for the achievement. The three generations of HiPP analyzers all base on the Scienta R4000 hemispherical analyzer with a pre-lens that contains differential pumping and electrostatic lenses. However, each design of pre-lens and the geometry of front aperture are different among these three HiPP systems [12, 24, 27]. As explained above, the first HiPP analyzer features a pre-lens of a relatively large acceptance angle and a 60° half-angle cone for enhanced photoelectron signal and differential pumping efficiency, respectively. This system has proven quite successful in many catalytic and electrocatalytic investigations at the gas–solid interfaces under in-situ and *operando* conditions [18, 19, 22, 28–31]. The HiPP-2 analyzer, for achieving efficient detection of high KE photoelectrons under more elevated pressures, is designed with the "swift acceleration lens mode" [32]. Not only does the HiPP-2 system advance our experimental capabilities in interfacial phenomena but also it brings this powerful surface/interface sensitive tool into fields of many intriguing liquid studies [21, 33, 34].

The HiPP-3 analyzer presented in this paper is a newly designed analyzer featuring an improved spatial resolution. To reduce the spherical aberration effects in conventional electron optics, a key strategy is to restrict the beam divergence and to keep electrons close to the optical axis for spatial resolution improvement. In the first HiPP design, this is obtained by moving the sample further away from the front aperture [14, 18]. But this method unavoidably results in a loss of signal due to this increase in distance where the photoelectrons travel in the elevated-pressure region. Taking advantage of the tightly focused beam spot at beamline 02B at SSRF, this HiPP-3 system instead introduces a novel "snap into place" aperture plate to

restrict the divergence of the beam bundle at a position further downstream of the lens. By this approach, the sample-to-aperture working distance (i.e., the focal point) is kept fixed regardless of the operation modes of transmission and imaging, which minimizes the travel distance of photoelectrons in the high-pressure region. Signal intensity and spatial resolution could be further optimized through different diameters of the "snap into place" apertures. Figure 2 shows the simulation of the photoelectron trajectories from the sample surface to the aperture of the hemispherical analyzer. The calculated spatial resolution under the best lens conditions could reach a total magnification of 32 times. A spatial resolution below 3 μm could in principle be achieved with this design in reducing the beam divergence. Employing the simulated lens table in our test, we have achieved a spatial resolution of 2.8 ± 0.3 μm in one dimension (see below).

3 Results and discussion

3.1 HiPP-3 performance in UHV measurements

We have evaluated the HiPP-3 analyzer performance in ultraviolet photoelectron spectroscopy (UPS) and XPS measurements under UHV with an ultraviolet light source and an aluminum X-ray source, respectively.

The UPS test is performed by measuring high-purity Xe gas (99.998%, Scienta GC50 gas cell) excited with a monochromatized helium lamp (He I, 21.2 eV) [35]. Figure 3a displays the Xe $5p_{3/2}$ spectrum acquired with the pass energy set to 5 eV and slit width 0.2 mm. The measured full width at half maximum (FWHM) is 4.9 meV. After deconvolution of the total excitation width and Doppler width of 3.4 meV [27, 35], the analyzer resolution is calculated to be 3.6 meV. The energy resolving power is over 1500 under 0.2 mm slit width setting and could be further improved with narrower slits.

The HiPP-3 analyzer performance in XPS is also evaluated by measuring Ag 3*d* core levels of a clean silver foil. Scienta MX650 source consisting of an Al anode unit and a quartz crystal monochromator was used as the excitation source, which delivers monochromatized X-ray at 1486.6 eV photon energy (Al Kα). Figure 3b reports the Ag $3d_{5/2}$ spectrum obtained on a clean silver foil (99.99%, Alfa Aesar) with 0.8 mm aperture diameter and 50 eV pass energy. The FWHM of the Ag $3d_{5/2}$ is measured to be 430 meV by fitting the spectrum with a Voigt function after a Shirley background subtraction. Considering the Lorentzian lifetime broadening of the photoinduced core hole (310 meV for Ag $3d_{5/2}$ transition [36]), the Gaussian contribution from the X-ray source (168 meV for MX650 [37]) and the Gaussian temperature broadening (90 meV [38]), one could estimate the broadening contribution from the HiPP-3 analyzer at this typical setting to be ∼ 113 meV [39]. Our UPS and XPS evaluations demonstrate that this APXPS system has sufficient energy resolution to support various surface physics and surface chemistry studies.

3.2 HiPP-3 performance at ambient pressure measurements

Using Al Kα X-ray source, the performance of the HiPP-3 analyzer over a broad energy range is demonstrated in Fig. 4. Under UHV and 2 mbar N_2 conditions, both Ag survey spectra show good statistics over the full KE range (Fig. 4a). It shows that the lens table is stable and shows a smooth transmission efficiency over a wide kinetic energy range. Ambient pressure measurements of Ag 3*d* core level peaks collected with 0.8 mm and 0.3 mm diameter apertures are shown in Fig. 4b, c, respectively. The wide

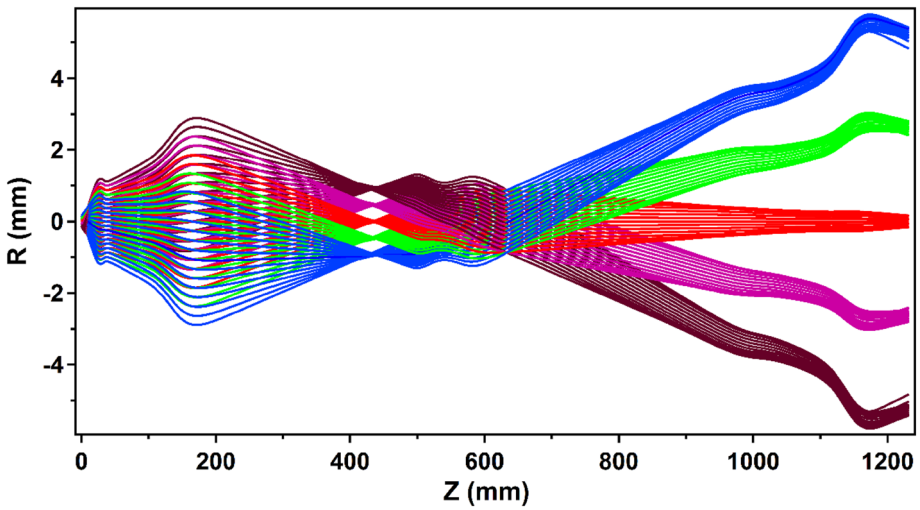

Fig. 2 (Color online) Simulation of the photoelectron trajectories. *X*-axis depicts the distance from the sample to the aperture of the hemispherical analyzer and *Y*-axis the distance from the axis of the analyzer

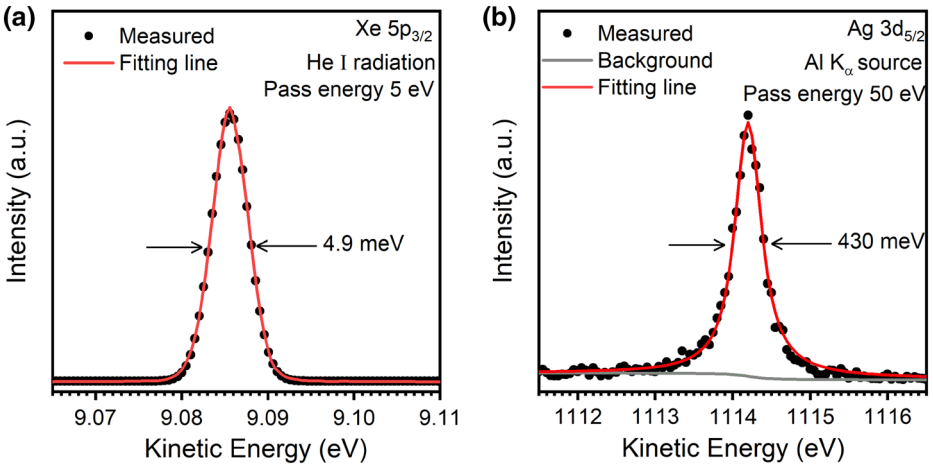

Fig. 3 (Color online) Analyzer performance test. **a** Xe $5p_{3/2}$ core level spectrum measured at 5 eV pass energy. The measured full width at half maximum (FWHM) is 4.9 meV. **b** Ag $3d_{5/2}$ core level spectrum with a FWHM of 430 meV

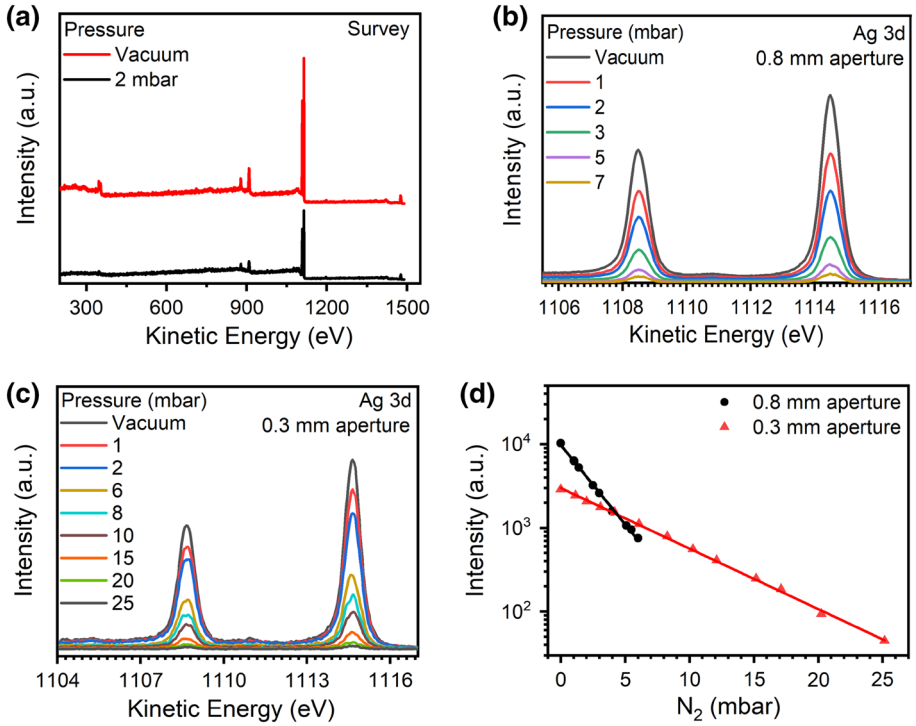

Fig. 4 (Color online) **a** The survey spectra of a Ag sample under UHV and 2 mbar N_2. Both spectra were collected at pass energy of 100 eV, energy step 0.5 eV and dwell time 0.2 s with 0.8 mm diameter aperture. **b** The Ag 3*d* spectra collected under different pressures with 0.8 mm aperture and **c** 0.3 mm aperture. **d** The Ag 3*d* peak intensity plotted as a function of N_2 pressure. All the spectra are collected using an Al Kα source

pressure range covering from UHV to 25 mbar N_2 validates the capability of this system for elevated pressure measurements. This pressure high limit of 25 mbar, close to the saturated vapor pressure of water at room temperature, stands more than a number but embodies the important ability to explore a lot of water-related systems. It is also worth noting that each spectrum is acquired within 60 s. The improved photoelectron detection efficiency under ambient conditions promises time-resolved studies with appropriate temporal resolution. In Fig. 4d, the Ag 3*d* peak intensity as a function of N_2 pressure is plotted. For the two aperture diameters investigated, the logarithm of Ag 3*d* peak intensity finds a linear decrease as the pressure increases, in good agreement with the electron attenuation in gas atmosphere [14]:

$$\ln(I/I_0) = -d_{\text{eff}}\sigma_e P/(kT) \quad (1)$$

where I/I_0 is the intensity ratio at a given pressure of P over the one at UHV, d_{eff} is the effective path length through gas and σ_e is the total electron scattering cross section. This indicates that the signal attenuation is solely due to the pressure increase and the analyzer brings no additional contributions, indicating stable and high electron transmission efficiency of this HiPP-3 analyzer from UHV to 25 mbar. Also, the rapid decrease in photoelectron intensity with the 0.8 mm diameter aperture and the intersection of

the two attenuation curves at ~ 4 mbar (Fig. 4d) give an benchmark on the selection of aperture diameter: a larger aperture is recommended at relatively lower pressures for maximizing signals, while a smaller one is preferred for higher pressure conditions (> 4 mbar in this case).

We have also tested the endstation up to 20 mbar pressure at the beamline. Figure 5a shows the Au 4f spectra measured under different pressures ranging from UHV to 20 mbar N_2 environment with the 0.3 mm diameter aperture at 1080 eV photon energy. The linear relationship between the logarithm of Au 4*f* intensity and the increasing pressure (not shown here) again demonstrates the stable and high electron transmission efficiency of HiPP-3 at the endstation. Interestingly, we observed a very small broadening of Au $4f_{7/2}$ peak with increasing pressure (Fig. 5b), which could be due to the increasing interactions between photoelectrons and gas molecules upon the increasing in gas pressure.

3.3 Imaging mode

The HiPP-3 hemispherical analyzer is equipped with two multi-channel plates and a charge-coupled device (CCD) camera. This detector system makes it possible to record data in two dimensions: one dimension gives the energy dispersion and the other the spatial distribution along the slit direction (shown in Fig. 6a). Lens tables have been developed for this imaging operation mode and are tested with both an Al Kα X-ray source and at the synchrotron beamline. In our first commissioning UHV test, we have obtained a spatial resolution of 2.8 ± 0.3 μm in one dimension. We expect that this spatial resolution can be improved with further optimization.

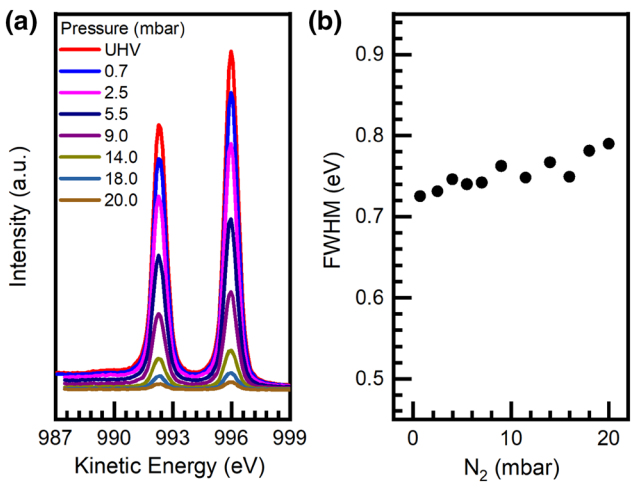

Fig. 5 (Color online) **a** The Au 4*f* spectra recorded at 1080 eV photon energy under different pressures from UHV to 20 mbar N_2 using the 0.3 mm diameter aperture. **b** The FWHM of the Au $4f_{7/2}$ peak as a function of pressure

Firstly, a sample consisting 40 μm Au lines on a Si wafer with 40 μm spacing (Fig. 6b) is measured using the Al Kα X-ray as excitation source under UHV. The sample is orientated in the way that the Au lines are perpendicular to the slit direction and a non-rotatable fixed sample manipulator is used. CCD images could be directly obtained and a representative one under UHV is shown in Fig. 6c. This image covers a field of ~ 800 μm at the Au $4d_{5/2}$ core level region. A typical XPS spectrum can be obtained by integrating a vertical slice of the CCD image at a given position while a horizontal slice of the image provides the spatial distribution of a given element (Au in this case). The trace in the top panel of Fig. 6d is obtained from the integrated intensities of the Au $4d_{5/2}$ photoemission signal in the range of 1146.0–1148.0 eV under UHV. The first derivative of this intensity plot is shown in the bottom panel of Fig. 6d. We here define the spatial resolution as the average FWHM of the derivative curve at the knife-edges. Under the testing condition of UHV, a spatial resolution of 2.8 ± 0.3 μm has been achieved. This is a significant improvement over the original HiPP system where a spatial resolution of 16 μm is reported [14].

At the beamline 02B at the SSRF, we have obtained a spatial resolution of 7.5 μm by measuring a sample (different from the above laboratory source experiment) with a similar sharp Au/Si edge under UHV. The Au thin film is prepared on Si wafer by photolithography. As shown in the scanned electron microscope image (Fig. 7a) the ~ 0.1 μm sharp edge ensures its width contributes negligibly in the spatial resolution measurement. Again, the sample is positioned such that the Au/Si edge is perpendicular to the slit direction. Figure 7b displays the CCD image of photoemission signal in the Au 4*f* and Si 2*p* region (KE of ~ 389–414 eV) obtained at 500 eV photon energy. The Au 4*f* and Si 2*p* signal well denotes the two regions, and the sharp edge is clearly delineated at − 0.13 mm. Integration of the Au $4f_{7/2}$ signal across the energy dispersion direction (from 411.5 to 413.0 eV) shows an abrupt intensity drop at the same position around − 0.13 mm (Fig. 7c). The first derivative of this intensity plot is reported in Fig. 7d. The FWHM of the derivative curve at − 0.13 mm is taken as a measure of the spatial resolution and estimated to be 7.5 μm in our test. This spatial resolution is not as good as the one obtained with the laboratory-based source. We attribute this difference to the vibration of the sample manipulation system employed in the endstation at the SSRF, which could be further optimized if needed.

As mentioned in the previous report [14], spectromicroscopy is an important tool for many in-situ studies. In this work, we have improved the spatial resolving capability of photoelectrons in one dimension. Yet, it is worth pointing out the challenges for a further improvement in

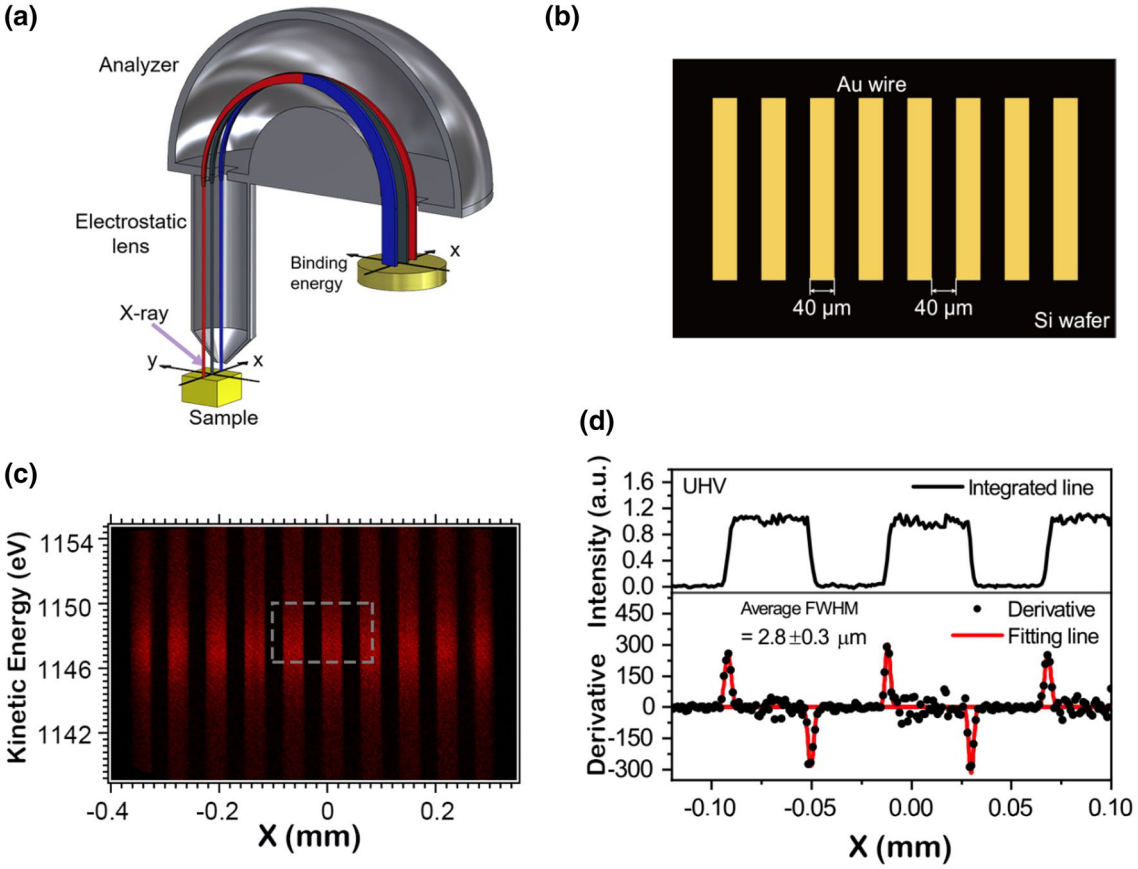

Fig. 6 (Color online) **a** Schematic of a two-dimensional detector. **b** Schematic of a sample consisting 40 μm Au lines on a Si wafer with 40 μm spacing. **c** Spatial resolved image of the Au $4d_{5/2}$ region covering multiple Au lines on the Si wafer under UHV. The KE values are plotted along the vertical axis and the position along the horizontal axis. **d** Top panel: the integrated Au $4d_{5/2}$ intensities within the gray dashed box in (**c**). Bottom panel: the first derivative of the integrated line, the average FWHM of which gives the spatial resolution of 2.8 ± 0.3 μm

the spatial resolution beyond micrometer into nanometer range using the current hemispherical energy analyzer. Other photoelectron-based in-situ techniques shall be considered for studies that require higher spatial resolution in the range of nanometers. For example, a recent report on near ambient pressure photoemission electron microscopy (PEEM) [40] has demonstrated high-resolution imaging under > 1 mbar. A spatial resolution better than 20 nm is achieved.

4 Conclusion

A new APXPS endstation has been designed and built at beamline 02B at the SSRF. By integrating a well-focused beam spot and a matching high-transmission HiPP-3 analyzer, we have demonstrated that this endstation can deliver good APXPS performance up to 30 mbar pressure and has potential in various gas–solid and liquid–solid in-situ/*operando* investigations. In additional, a well-improved spectromicroscopy capability is achieved at this endstation with a spatial resolution of 2.8 ± 0.3 μm in one dimension. More importantly, many of the endstation design features are tailored to provide solutions for scientific problems of interest, such as exchangeable aperture cones for different experimental requirements, easy sample transfer for liquid studies as well as high adaptability in setup modifications for electrochemical systems. This is our effort to apply a rational design and to improve a user endstation performance by taking into account the beamline specifics and the scientific goals together. By doing so, we hope that this endstation will be another useful and versatile tool for in-situ interfacial phenomena explorations.

Currently, several synchrotron facilities have constructed beamlines specifically designed to combine APXPS endstations with other characterization techniques to provide multimodal tools to users, such as the Energy Materials In-situ Laboratory Berlin (EMIL) at BESSY II [41] and the Versatile Soft X-ray beamline (VERSOX) at

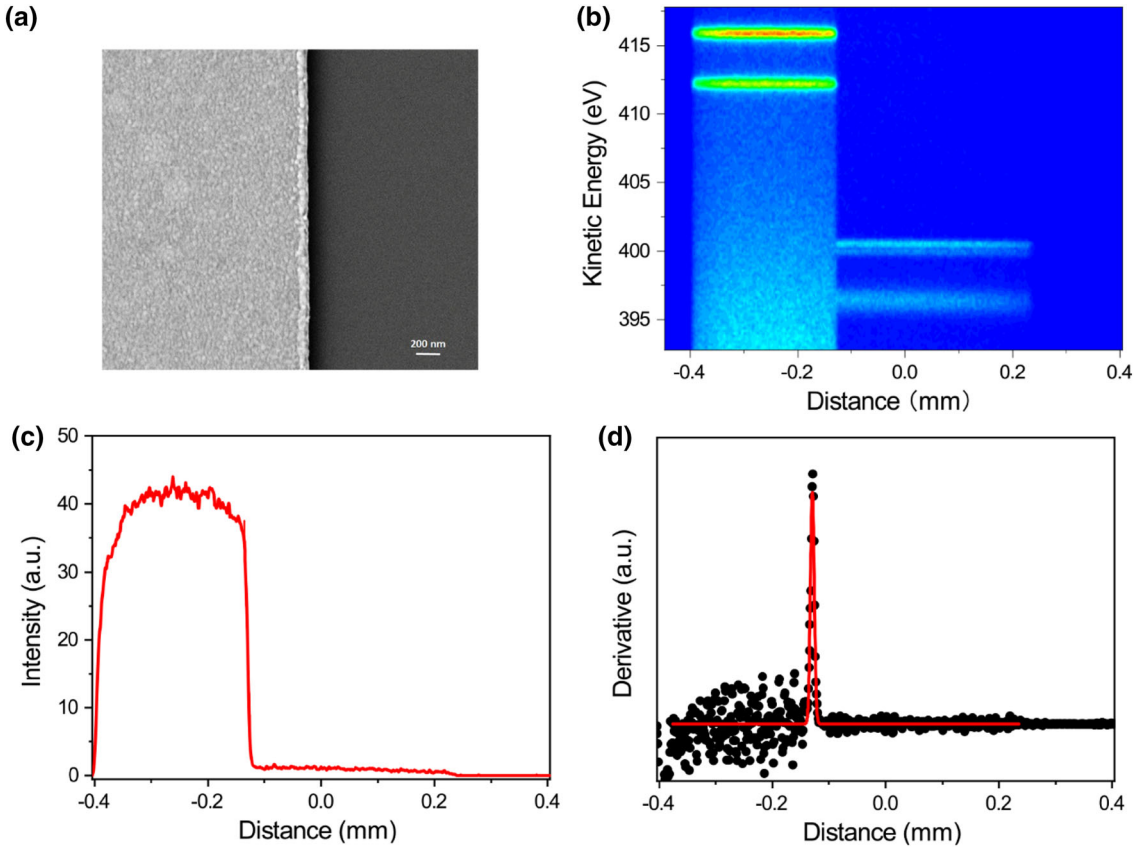

Fig. 7 (Color online) **a** Scanned electron microscope image of the Au/Si sample. **b** CCD image of Au 4*f* and Si 2*p* photoemission near the Au/Si edge. **c** The integrated Au $4f_{7/2}$ intensities versus position. **d** The first derivative of the curve in **c**, the FWHM of which gives the spatial resolution of 7.5 μm

Diamond Light Source [42]. These endstations are designed and capable of applying several characterization techniques under different environments simultaneously across a wide photon energy range. Our endstation is also part of a new beamline project, ME^2 (Materials for Energy and Environment beamline), which combines most of the soft X-ray in-situ characterization techniques (XPS, X-ray absorption spectroscopy (XAS) and X-ray emission spectroscopy (XES)) with in-situ material growth capability. The goal of the ME^2 beamline is to close the discovery loop and facilitate the rational design of the next generation energy materials [43]. This beamline project has finished and is now opened to users.

References

1. G.A. Somorjai, Y. Li, *Introduction to Surface Chemistry and Catalysis* (Wiley, Hoboken, 2010)
2. S. Hüfner, *Photoelectron spectroscopy: principles and applications* (Springer, Berlin, 2013)
3. M. Salmeron, R. Schlögl, Ambient pressure photoelectron spectroscopy: a new tool for surface science and nanotechnology. Surf. Sci. Rep. **63**(4), 169–199 (2008). https://doi.org/10.1016/j.surfrep.2008.01.001
4. D. Starr, Z. Liu, M. Hävecker et al., Investigation of solid/vapor interfaces using ambient pressure X-ray photoelectron spectroscopy. Chem. Soc. Rev. **42**(13), 5833–5857 (2013). https://doi.org/10.1039/C3CS60057B
5. H.-J. Freund, H. Kuhlenbeck, J. Libuda et al., Bridging the pressure and materials gaps between catalysis and surface science: clean and modified oxide surfaces. Top. Catal. **15**(2–4), 201–209 (2001). https://doi.org/10.1023/A:1016686322301
6. P. Stoltze, J. Nørskov, Bridging the "Pressure Gap" between ultrahigh-vacuum surface physics and high-pressure catalysis. Phys. Rev. Lett. **55**(22), 2502–2505 (1985). https://doi.org/10.1103/PhysRevLett.55.2502
7. K. Siegbahn, C. Nordling, G. Johansson et al., *ESCA Applied to Free Molecules* (North-Holland Publishing Co., Amsterdam, 1969)
8. R.W. Joyner, M.W. Roberts, K. Yates, A "high-pressure" electron spectrometer for surface studies. Surf. Sci. **87**(2), 501–509 (1979). https://doi.org/10.1016/0039-6028(79)90544-2
9. H. Siegbahn, S. Svensson, M. Lundholm, A new method for ESCA studies of liquid-phase samples. J. Electron Spectrosc. Relat. Phenom. **24**(2), 205–213 (1981). https://doi.org/10.1016/0368-2048(81)80007-2
10. H. Ruppender, M. Grunze, C. Kong et al., In situ X-ray photoelectron spectroscopy of surfaces at pressures up to 1 mbar. Surf. Interface Anal. **15**(4), 245–253 (1990). https://doi.org/10.1002/sia.740150403

11. D.F. Ogletree, H. Bluhm, G. Lebedev et al., A differentially pumped electrostatic lens system for photoemission studies in the millibar range. Rev. Sci. Instrum. **73**(11), 3872–3877 (2002). https://doi.org/10.1063/1.1512336
12. D.F. Ogletree, H. Bluhm, E.D. Hebenstreit et al., Photoelectron spectroscopy under ambient pressure and temperature conditions. Nucl. Instrum. Methods A **601**(1), 151–160 (2009). https://doi.org/10.1016/j.nima.2008.12.155
13. H. Bluhm, M. Hävecker, A. Knop-Gericke et al., Methanol oxidation on a copper catalyst investigated using in situ X-ray photoelectron spectroscopy. J. Phys. Chem. B **108**(38), 14340–14347 (2004). https://doi.org/10.1021/jp040080j
14. M.E. Grass, P.G. Karlsson, F. Aksoy et al., New ambient pressure photoemission endstation at Advanced Light Source beamline 9.3.2. Rev. Sci. Instrum. **81**(5), 053106 (2010). https://doi.org/10.1063/1.3427218
15. J. Schnadt, J. Knudsen, J.N. Andersen et al., The new ambient-pressure X-ray photoelectron spectroscopy instrument at MAX-lab. J. Synchrotron. Radiat. **19**(5), 701–704 (2012). https://doi.org/10.1107/S0909049512032700
16. R. Toyoshima, M. Yoshida, Y. Monya et al., In situ ambient pressure XPS study of CO oxidation reaction on Pd(111) surfaces. J. Phys. Chem. C **116**(35), 18691–18697 (2012). https://doi.org/10.1021/jp301636u
17. S. Kaya, H. Ogasawara, L.-Å. Näslund et al., Ambient-pressure photoelectron spectroscopy for heterogeneous catalysis and electrochemistry. Catal. Today **205**, 101–105 (2013). https://doi.org/10.1016/j.cattod.2012.08.005
18. C. Zhang, M.E. Grass, A.H. McDaniel et al., Measuring fundamental properties in operating solid oxide electrochemical cells by using in situ X-ray photoelectron spectroscopy. Nat. Mater. **9**(11), 944–949 (2010). https://doi.org/10.1038/nmat2851
19. F. Tao, M.E. Grass, Y. Zhang et al., Reaction-driven restructuring of Rh-Pd and Pt-Pd core-shell nanoparticles. Science **322**(5903), 932–934 (2008). https://doi.org/10.1126/science.1164170
20. G.A. Somorjai, H. Frei, J.Y. Park, Advancing the frontiers in nanocatalysis, biointerfaces, and renewable energy conversion by innovations of surface techniques. J. Am. Chem. Soc. **131**(46), 16589–16605 (2009). https://doi.org/10.1021/ja9061954
21. M. Favaro, B. Jeong, P.N. Ross et al., Unravelling the electrochemical double layer by direct probing of the solid/liquid interface. Nat. Commun. **7**, 12695 (2016). https://doi.org/10.1038/ncomms12695
22. N.J. Divins, A. Inma, E. Carlos et al., Influence of the support on surface rearrangements of bimetallic nanoparticles in real catalysts. Science **346**(6209), 620–623 (2014). https://doi.org/10.1126/science.1258106
23. S. Axnanda, E.J. Crumlin, B. Mao et al., Using "Tender" X-ray ambient pressure X-ray photoelectron spectroscopy as a direct probe of solid-liquid interface. Sci. Rep. **5**, 9788 (2015). https://doi.org/10.1038/srep09788
24. S.K. Eriksson, M. Hahlin, J.M. Kahk et al., A versatile photoelectron spectrometer for pressures up to 30 mbar. Rev. Sci. Instrum. **85**(7), 075119 (2014). https://doi.org/10.1063/1.4890665
25. D. Teschner, A. Pestryakov, E. Kleimenov et al., High-pressure X-ray photoelectron spectroscopy of palladium model hydrogenation catalysts: part 1: effect of gas ambient and temperature. J. Catal. **230**(1), 186–194 (2005). https://doi.org/10.1016/j.jcat.2004.11.036
26. S. Nemšák, E. Strelcov, H. Guo et al., In aqua electrochemistry probed by XPEEM: Experimental setup, examples, and challenges. Top. Catal. **61**(20), 2195–2206 (2018). https://doi.org/10.1007/s11244-018-1065-4
27. N. Mårtensson, P. Baltzer, P.A. Brühwiler et al., A very high resolution electron spectrometer. J. Electron Spectrosc. Relat. Phenom. **70**(2), 117–128 (1994). https://doi.org/10.1016/0368-2048(94)02224-N
28. F. Tao, S. Dag, L.-W. Wang et al., Break-up of stepped platinum catalyst surfaces by high CO coverage. Science **327**(5967), 850–853 (2010). https://doi.org/10.1126/science.1182122
29. P. Gao, S. Li, X. Bu et al., Direct conversion of CO_2 into liquid fuels with high selectivity over a bifunctional catalyst. Nat. Chem. **9**(1), 1019–1024 (2017). https://doi.org/10.1038/nchem.2794
30. C. Zhang, M.E. Grass, Y. Yu et al., Multielement activity mapping and potential mapping in solid oxide electrochemical cells through the use of operando XPS. ACS Catal. **2**(11), 2297–2304 (2012). https://doi.org/10.1021/cs3004243
31. C. Zhang, Y. Yu, M.E. Grass et al., Mechanistic studies of water electrolysis and hydrogen electro-oxidation on high temperature ceria-based solid oxide electrochemical cells. J. Am. Chem. Soc. **135**(31), 11572–11579 (2013). https://doi.org/10.1021/ja402604u
32. M.O.M. Edwards, P.G. Karlsson, S.K. Eriksson et al., Increased photoelectron transmission in High-pressure photoelectron spectrometers using "swift acceleration". Nucl. Instrum. Methods A **785**, 191–196 (2015). https://doi.org/10.1016/j.nima.2015.02.047
33. Y. Han, S. Axnanda, E.J. Crumlin et al., Observing the electrochemical oxidation of Co metal at the solid/liquid interface using ambient pressure X-ray photoelectron spectroscopy. J. Phys. Chem. B. (2017). https://doi.org/10.1021/acs.jpcb.7b05982
34. M.F. Lichterman, S. Hu, M.H. Richter et al., Direct observation of the energetics at a semiconductor/liquid junction by operando X-ray photoelectron spectroscopy. Energy Environ. Sci. **8**(8), 2409–2416 (2015). https://doi.org/10.1039/C5EE01014D
35. P. Baltzer, L. Karlsson, M. Lundqvist et al., Resolution and signal-to-background enhancement in gas-phase electron spectroscopy. Rev. Sci. Instrum. **64**(8), 2179–2189 (1993). https://doi.org/10.1063/1.1143957
36. J.L. Campbell, T. Papp, Widths of the atomic K-N7 levels. Atomic Data Nucl. Data Tables **77**(1), 1–56 (2001). https://doi.org/10.1006/adnd.2000.0848
37. H. Fellner-Feldegg, Ph.D. dissertation, Uppsala University, 1974
38. S. Mähl, M. Neumann, S. Dieckhoff et al., Characterisation of the VG ESCALAB instrumental broadening functions by XPS measurements at the Fermi edge of silver. J. Electron Spectrosc. Relat. Phenom. **85**(3), 197–203 (1997). https://doi.org/10.1016/S0368-2048(97)00074-1
39. J.J. Olivero, R.L. Longbothum, Empirical fits to the Voigt line width: a brief review. J. Quant. Spectrosc. Radiat. Transf. **17**(2), 233–236 (1977). https://doi.org/10.1016/0022-4073(77)90161-3
40. Y. Ning, Q. Fu, Y. Li et al., A near ambient pressure photoemission electron microscope (NAP-PEEM). Ultramicroscopy **200**, 105–110 (2019). https://doi.org/10.1016/j.ultramic.2019.02.028
41. R. Follath, M. Hävecker, G. Reichardt, K. Lips, J. Bahrdt, F. Schäfers and P. Schmid, presented at the Journal of Physics: Conference Series, 2013 (unpublished)
42. G. Materlik, T. Rayment, D.I. Stuart, Diamond light source: status and perspectives. Philos. Trans. A Math. Phys. Eng. Sci **373**(2036), 20130161 (2015). https://doi.org/10.1098/rsta.2013.0161
43. X. Liu, W. Yang, Z. Liu, Recent progress on synchrotron-based in-situ soft X-ray spectroscopy for energy materials. Adv. Mater. **26**(46), 7710–7729 (2014). https://doi.org/10.1002/adma.201304676